Indian Journal of Biochemistry & Biophysics
Vol. 41, December 2004, pp. 311-321

Phonon dispersion in polyinosinic acid

Seema Srivastava, Shinoo Srivastava, Irfan Ali Khan, M K Pandey and V D Gupta*
Department of Physics, Integral University, Kursi Road, Lucknow 226 026, India

Received 30 July 2004; revised 25 October 2004

A study of the normal modes of vibration and their dispersion in polyinosinic acid [poly (I)] along the helix axis based on Urey-Bradley force field is reported. It leads to a better interpretation of Raman and FTIR spectra. A comparison of dispersion curves of poly (I) with poly (G) has been made. Characteristic features of dispersion curves, such as regions of high density-of-states, repulsion and character mixing are discussed. Predictive value of heat capacity as a function of temperature is reported.

Keywords: Normal modes, dispersion curves, Fourier transform, density-of-states, polyinosinic acid

The nucleic acids, like polypeptides possess a variety of polymorphic forms, other than the originally assumed in Watson and Crick model. These include A, B, Z, right-handed and parallel-stranded duplex hairpin with ordered loops, triplexes and quadruplexes[1-16]. Many of these polymorphs are stabilized by non-Watson and Crick base-base and base-backbone interactions and some of them are very interesting and unusual. For example, the guanine quadruplex motif has DNA sequences with stretches of guanine residues, capable of forming the four-stranded structure occurring at the ends of eukaryotic chromosomes, the telomeres. Polyinosinic [poly(I)], polythymidilic, and polycytidilic acids also form hydrogen bonded four-stranded structures, as confirmed by circular dichroism[4], though they are not a part of the chromosomes like as guanine-rich DNAs.

Vibrational dynamics is a powerful tool[16] for understanding the dynamical and thermodynamical behaviour of molecular and macromolecular systems (long chain) and their conformational dependence. For example, vibrational dynamics of a simple polypeptide, such as polyglycine is entirely different from glycine; conformationally, polyglycine II is a three-fold helical system, whereas glycine is a simple molecular system. The thermodynamic behaviour of a polyglycine chain will depend on the profile of dispersion curves, whereas glycine molecule cannot be treated as a one-dimensional infinite system and hence there is no dispersive behaviour of the vibrations. Thus, the dynamics of an infinite system is an order of magnitude more different and involved, as compared with finite molecules. Earlier, vibrational dynamics was used to study a large number of polymeric systems, synthetic as well as of biological importance[17-20]. Here, we report vibrational studies on poly(I), which at low salt concentration (0.01 *M* Na^+) exists as a single-stranded species in the aqueous solution. At this concentration, it has an appreciable ordered structure, however, at higher concentration, it becomes self associated into a stable multi-stranded structure[21].

X-ray diffraction study[22] has shown that at higher ionic concentration the structure of poly(I) (Fig.1) is very similar to associated polyguanylic acid; poly(I) fibers favoured a right-handed model, in which four parallel strands are linked by inter-base N_1-H…O_6 hydrogen bonds, with C_2'- or C_3'-endo conformation of the furanose ring. However, spectroscopic and molecular modelling studies[23-25] on poly(I) suggest that it belongs to the A-type family of nucleic acids characterized by C_3'-endo ribose conformation. Further, the presence of metal ions is reported to be essential for the formation of four-stranded helical complexes of poly (I); their stabilizing effect being related to their ability to fill the central hole of the tetrameric basic units. Although the vibrational spectra of poly(I) in its complete tetrameric form has been is reported earlier[21], the full dispersion of normal modes, which is essential for a fuller understanding of the spectral features and thermodynamic behaviour has not been reported, so far. In the present paper, the

*To whom all correspondence should be addressed
Phone: +91(0522) 2890812, 2890730, 3096117;
Fax: 0522-2890809, 2310778
E-mail: vdg1@rediffmail.com/vdgupt@yahoo.co.in

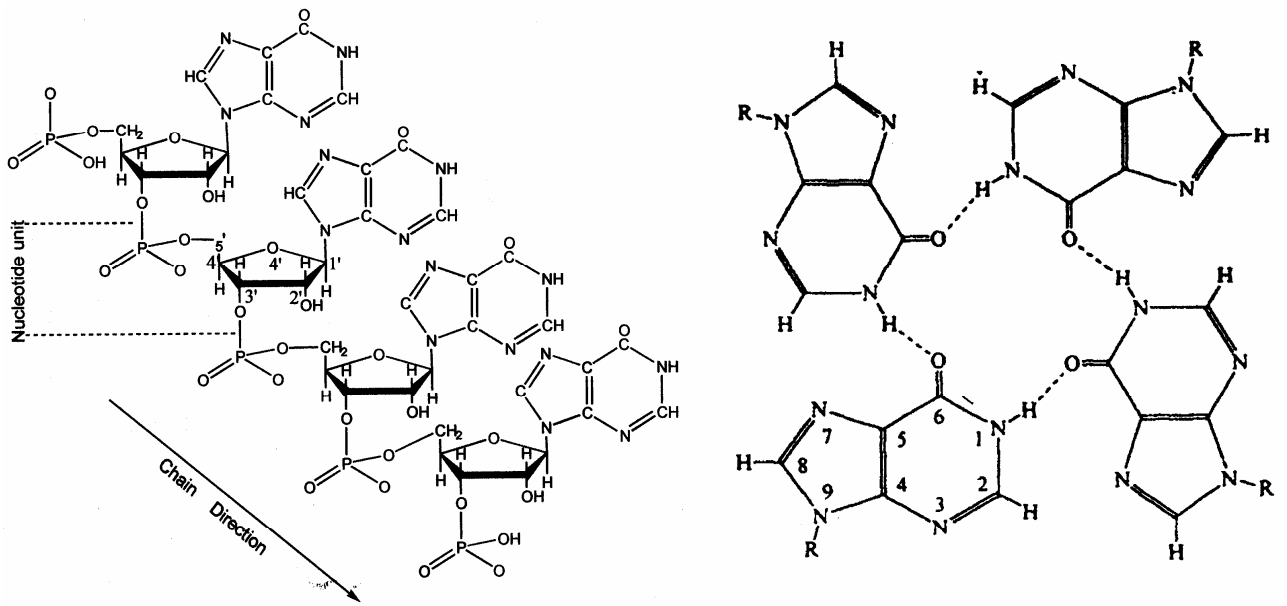

Fig. 1—(A): Chemical repeat unit and internal coordinates of poly (I); and (B): basic unit of the four-stranded helical complex of poly (I)

normal modes and their dispersion along the chain axis, density-of-states and heat capacity for poly (I) are reported. The Urey-Bradley potential field is used for intramolecular interactions[26].

Theory and Experiment

Normal mode calculation

The normal mode frequencies were calculated according to the Wilson's *GF*[27] matrix method, as modified by Higgs[28]. It consists of writing the inverse kinetic energy matrix G and the potential energy matrix F in terms of internal coordinates R. For an infinite isolated helical polymer, an infinite number of internal coordinates lead to G and F matrices of infinite order. Due to the screw symmetry of a polymer, a transformation similar to that given by Born and von Karman[29] can be performed that reduces the infinite problem to finite dimensions[29]. The vibrational secular equation, which provides normal mode frequencies and their dispersion as a function of phase angle has the form:

$$G(\delta)F(\delta) - \lambda(\delta) I = 0,\ 0 \le \delta \le \pi \qquad \ldots(1)$$

where G is the inverse of kinetic energy matrix, F is the potential field matrix. Both are written in internal coordinate system and are a function of the phase relation δ between the successive residues I is the unit matrix. The vibrational frequencies $\nu(\delta)$ (in cm^{-1}) are related to the eigen values $\lambda(\delta)$ by the following relation:

$$\lambda(\delta) = 4\pi^2 c^2 \nu^2(\delta) \qquad \ldots(2)$$

where c is the velocity of light. This methodology is well established and has been successfully adopted to interpret the spectra of a large number of polymers[17-19] such as polypeptides, polyethylene, polyvinylchloride, polyacetelyne, poly (L-valine)[19]. Although the selection rules for finite systems (oligomers) are quite different from an infinite system, the dispersion curves can be mapped with the help of IR/Raman/Inelastic neutron scattering peaks in the spectra[19] of oligomers. This relationship between the dynamics of finite and infinite systems has been well established in case of polyglycine/poly (L-valine) etc[19]. In the present work, the variation of phase angle from 0 to π (or helix angle) provides the local as well as the global features.

Force field

Several types of force field have been used for the study of structural, energetic and dynamical behaviour of molecules[26] and choice of a particular field depends very much on one's experience and chemical intuition. Vibrational frequencies are very sensitive to the accuracy of the potential field and these are usually known to within, say 2 cm^{-1}. In the present study, the Urey-Bradley force field, which has some advantages over other fields has been used. It takes into account both bonded and non-bonded interactions as well as internal tension and there are no cross terms in the expression for energy[29, 30].

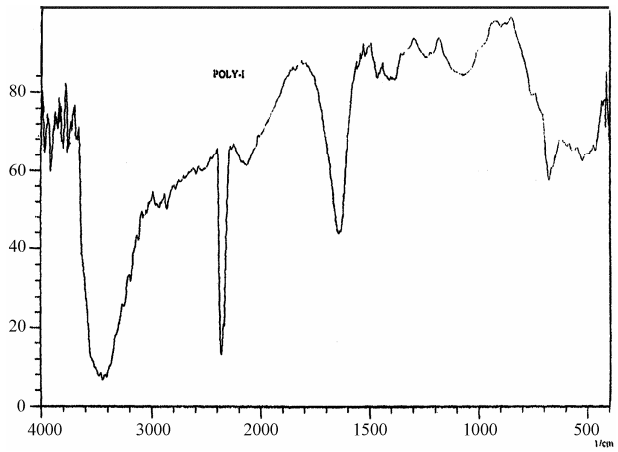

Fig. 2—FTIR spectra of poly(I) (4000-450 cm^{-1})

For error analysis, the force constant moment matrix M (F) can be obtained from:

$$M(F) = \sigma^2 (Z^+ J^+ PJZ) \quad \ldots(3)$$

where $\sigma^2 = [(\Delta\lambda)^+ P (\Delta\lambda)]/d$, P is the matrix of weighting factors, d is the number of degrees of freedom, $\Delta\lambda$ are corrections in eigen frequencies, J is computed from the initial eigen functions L_0Z is the matrix related to force field matrix. The diagonal elements of M(F) give the uncertainties in the calculated force constants and the off diagonal elements give the correlation between the errors in force constants. As these matrices are of large dimensions, their reproduction will consume lot of space and hence is not been given here. However, through the "goodness of fit" (ratio of variances), one can also judge the stability and validity of the force constant parameters. For the present model, it is significantly low ($p<001$). The coefficient of multiple correlation (R^2) is very high (1000). The values of residual sum of squares (3686258), mean sum of squares (24575050) and F (510798) show that the fitting is highly significant. By changing assignments and initial set of constants, further check on the uniqueness of force constant parameters was made which invariably led to several abnormal values. Any other set of force constants led to non-convergence of parameters. Thus, the various approaches indicate towards stability and unique character of force constants.

The volume heat capacity (C_v) has been obtained from the dispersion curves via density-of-states and converted into constant pressure heat capacity (C_p) using the Nernst-Lindemann approximation[29,31,32].

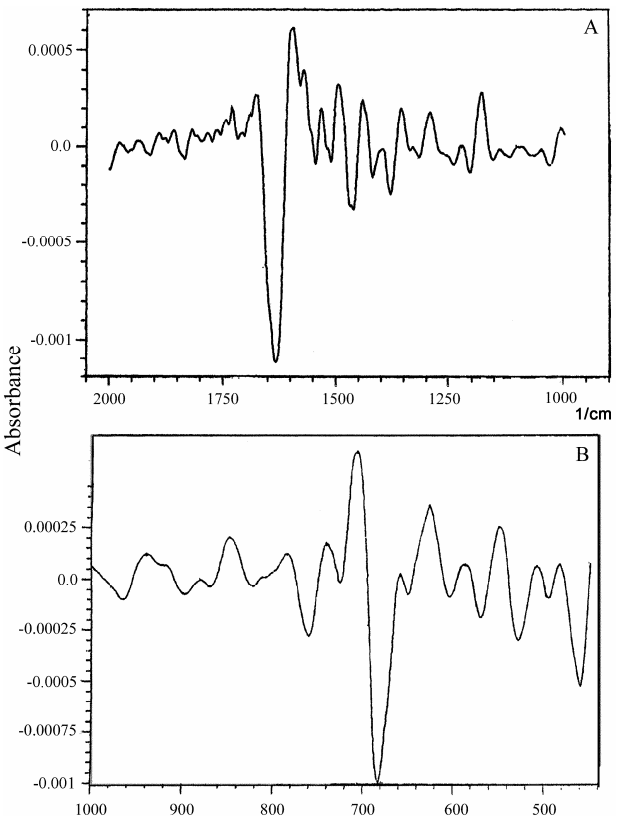

Fig. 3—(A): Second derivative spectra of poly(I) (2000-1000 cm^{-1}); and (B) second derivative spectra of poly(I) (1000-450 cm^{-1})

Experiment

The FTIR spectra and its second derivative of poly(I) obtained from Sigma Chemicals (sigma@del2vsnlnetin) has been recorded on a Shimadzu 8201 PC Fourier transform spectro photometer in the range 4000-450 cm^{-1} at a resolution better than 1 cm^{-1}. Before running the spectra, the equipment was well purged with dry nitrogen. The sample was in the solid state and the spectra were obtained in CsBr pellet. IR spectra and its second derivative are shown in Figs 2 and 3. The Raman spectra of Simard and Savoie[21] have been used.

Results and Discussion

In order to reduce the dimensions of the problem to a manageable size, the masses of hydrogen atoms attached to the skeletal as well as side chain atoms have been added to the parent atoms to which they are attached, thus ignoring the degree of freedom associated with these atoms. In other words, we can say that during normal vibrations the motions involving hydrogen atoms are uncoupled from the motion of the nearest neighbours or the rest of the

structure and the hydrogen atoms remain rigidly fixed to their atoms of attachment. This approximation would not materially affect the vibrations below 700 cm^{-1} which are of dispersive nature. Further, the C-H stretch and in-plane and out-of-plane bends are highly localized modes. Under this approximation the number of atoms per residue in poly(I) is 22 and hence there would be 22 × 3-4 = 62 normal modes of vibrations. The vibrational frequencies have been calculated for values of δ varying from 0 to π in steps of 0.05 π and the optically active modes are those for which δ = 00, 0.18 π and 0.36 π. The first two are IR-active, but all are Raman-active. The four zero frequencies correspond to acoustic modes, three representing translations along the three axes and one is rotation of the chain around the chain axis.

The assignments have been made on the basis of potential energy distribution (PED), energy of absorption, band shape, band intensity, derivative spectra, and absorption/scattering in similar molecules having groups placed in similar environments. Full use has been made of the spectral information available in the literature. The Urey-Bradley[26] force constants were initially transferred from our earlier work on poly(U)[17] and were further refined by using the least-square fit method as described earlier[17]. Final set of force constants for poly(I) is given in Table 1 and except for a couple of frequencies, most of the frequencies are fitted within less than 1%. As mentioned earlier, the modes corresponding to δ = 0.0 are both Raman and IR-active. Therefore, the observed frequencies are first fitted to the calculated frequencies at this phase value. The remaining observed frequencies in Raman/IR spectra correspond to the frequencies lying on the intersect at $\delta = 0.18\pi$ and 0.36 π (Raman only) as shown in Figs 4-7. The dispersion curves below 900 cm^{-1} are shown in Figs 4(a), 5(a), 6(a) and 7(a). All backbone, side chain and mix modes along with their PEDs are given in Tables 2, 3 and 4 respectively. Since hydrogen atoms have merged in the parent atom, frequencies involving the hydrogen atom do not appear in our calculations and are not given.

Backbone modes

The modes, involving the motion of sugar ring and phosphate atoms (C=O, C-C, P-O stretches, O-P-O bendings and their mixtures) and termed as backbone modes are given in Table 2. The stretching of phosphate group as reported earlier is the most discussed mode[17]. For example, in A-DNA, the mode, which appears at 1090 cm^{-1} due to symmetric stretching of PO_4 group shifts to 1098 cm^{-1} in poly(U)[17]. In the present case, a broad and asymmetric band with its maximum at 1234 cm^{-1} has been assigned to the asymmetric stretching motion of the PO_4 group and the corresponding symmetric stretch has been assigned at 1099 cm^{-1} in IR and 1091 cm^{-1} in Raman spectra. The calculated values are in good agreement with the observed ones. As proposed by Watson and Crick[33], based on the X-ray studies that O-----O line is perpendicular to the helix axis and the bisector of the angle O-P-O is almost parallel to the fiber axis. This orientation should give rise to the perpendicular dichroism in the band assigned to the PO_2 asymmetric stretch vibration at 1234 cm^{-1} and parallel dichroism in the band assigned to the PO_2^- symmetric stretching vibration at 1099 cm^{-1} (observed in Raman spectra at 1091 cm^{-1}). The anti-symmetric stretching of phosphate group in other polynucleotides[33] generally occurs, as a sharp mode around 1240 cm^{-1}. The sharpness of absorption band indicates that it is an independent mode. Its occurrence as a shoulder at 1207 cm^{-1} indicates that in poly(I) PO_2 anti-symmetric stretch does not take place independently. The calculations indicate that the PO_2 group modes interact strongly with each other in the chain, which complicates its structure; consequently, the spectral features become both broad and asymmetric.

The fact that four stranded poly(I) exhibits an A-type helix geometry characterstic of the ribonucleic acids (C3′-endo conformation), rather than B-type structure[25] is also reflected in our calculations. For example, the band occurring in the range 830-810 cm^{-1} in polynucleotides arises from the vibrations of the phosphate sugar portions of the molecule and provides a sensitive handle for the diagnosis of backbone conformation of the polymer. In the present study, a composite band is observed at 826 cm^{-1}, with a shoulder at 810 cm^{-1} in the second derivative spectra. It has been reported that in case of C2′-endo conformation, this band occurs at higher frequency of approximately at 835 cm^{-1}. The composite band observed at lower frequency as in our case is a characteristic of C3′-endo conformation[17]. This mode is calculated at 819 cm^{-1}, showing PED only from sugar ring and phosphate group vibrations. The other characteristic vibration of nucleotides is OPO of phosphate group. Nine modes corresponding to this

Table 1—Internal coordinates and force constants (md A^{-1})

Int. coord. stretches	Force constant value	Int. coord. in-plane bendings	Force constant value		Int. coord. out-of-plane bendings	Force constant value
			Bonded	Non-bonded		
ν(P-O)	2.40	ϕ (O-P=O)	1.4300	(0.50)	ω(PO)	0.200
ν(P=O)	7.35	ϕ (O-P-O)	1.0700	(0.50)	ω(C6O6)	0.120
ν(OC5')	2.45	ϕ (O=P=O)	1.3300	(0.60)	ω(C2'O)	0.300
ν(C5'C4')	3.60	ϕ(POC5')	0.9500	(0.30)	τ(N9C8)	0.050
ν(CC)s	2.30	ϕ (OC5'C4')	0.5000	(0.50)	τ(P-O)	0.010
ν(C4'/C1',O4')	2.55	ϕ (C5'C4'C3')	0.4008	(0.20)	τ(OC5')	0.010
ν(C3'O)	9.35	ϕ (C5'C4'O4')	0.3500	(0.50)	τ(C5'C4')	0.050
ν(C2'O)	4.82	ϕ (CCO)s	0.5000	(0.50)	τ(CC)s	0.010
ν(N9,C1'/C8)	2.99	ϕ (CCC)s	0.5000	(0.20)	τ(C1'/C4'O)s	0.010
ν(NC)i	4.20	ϕ (C4'/C2'C3'O	0.2000	(0.25)	τ(N9C1')	0.050
ν(C4C5)i	6.50	ϕ (C3'/C1'C2'O)	0.5000	(0.50)	τ(N9C4)	0.050
ν(N=C)	3.50	ϕ (C2'C1'N9)	0.5500	(0.50)	τ(C4C5)	0.020
ν(C5C6)	2.90	ϕ (O4'C1'N9)	0.4000	(0.50)	τ(N=C)	0.060
ν(C6O6)	9.50	ϕ (C1'O4'C4'	0.4500	(0.55)	τ(C5C6)	0.025
ν(C6/C2,N1)	5.05	ϕ (C1'N9C4)	0.4000	(0.50)	τ(C6N1)	0.039
ν(C2N1)	5.05	ϕ (C1'N9C8)	0.4000	(0.55)	τ(C2N1)	0.039
		ϕ (C4N9C8)	0.6500	(0.55)	τ(C3'O)	0.020
		ϕ (NCC)i	0.4000	(0.20)		
		ϕ (N9C4N3)	0.6000	(0.55)		
		ϕ (C4C5C6)	0.5000	(0.20)		
		ϕ (N7C5C6)	0.5000	(0.25)		
		ϕ (C5N7C8)	0.7000	(0.55)		
		ϕ (N7C8N9)	0.5000	(0.55)		
		ϕ (C5C6O6)	0.9500	(0.50)		
		ϕ (C5C6N1)	0.5000	(0.20)		
		ϕ (O6C6N1)	0.3800	(0.90)		
		ϕ (C6N1C2)	0.5500	(0.55)		
		ϕ (N1C2N3)	0.6000	(0.55)		
		ϕ (C2N3C4)	0.9500	(0.55)		
		ϕ (C3'OP)	0.3500	(0.25)		

ν, ϕ, ω, and τ represent stretch, angle bends, wags and torsions respectively. s, i outside side the parantheses and for sugar ring and inosinic acid respectively.

mode in the range of 683-471 cm^{-1} have been calculated and their values are in good agreement with the observed ones.

Side chain modes

The 1600 cm^{-1} region of the spectra of poly(I) is of special importance, as it reflects the state of carbonyl groups, which are directly involved in the formation of hypoxanthine quartets. Earlier, a multiplet structure resulting from the coupled stretching vibrations of the four C=O groups within each tetramer was proposed[21] and assuming a local C_{4h} symmetry, the high frequency component at 1721 cm^{-1} and a less intense band at 1689 cm^{-1} were assigned to the Raman active component of Ag and Bg symmetry, respectively. In the present case, the intense peak observed at 1641 cm^{-1} arises probably due to the fact that (C_2'O) has a weak shoulder at 1694 cm^{-1}, which is clearly resolved in the second derivative into three components at 1720, 1706 and 1691 cm^{-1}. This shoulder has been assigned to the (C=O) stretching vibration.

Dispersion curves

The dispersion curves below 850 cm^{-1} are shown in Figs 4(a), 5(a), 6(a) and 7(a). The modes above 800 cm^{-1} are either non-dispersive or their dispersion is less than 5 cm^{-1}. One of the characteristic features of the dispersion curves is the divergence observed

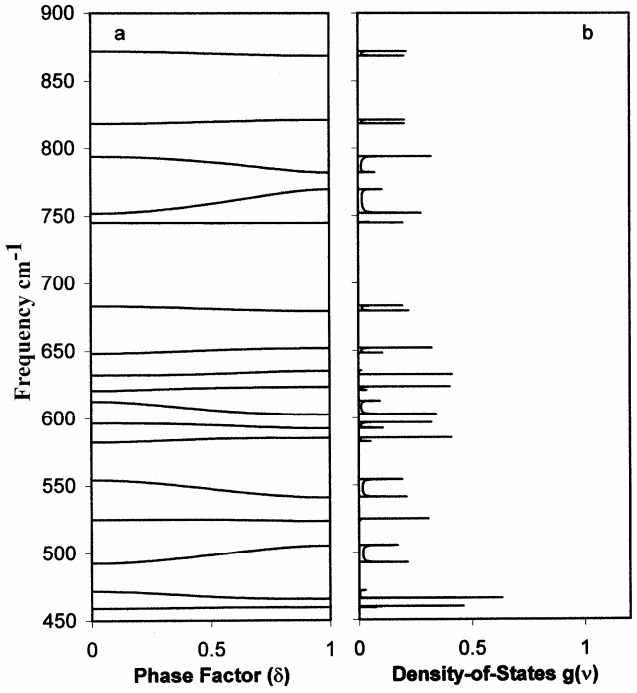

Fig. 4—Dispersion curves (a) and (b) of poly (I) (500-900 cm^{-1})

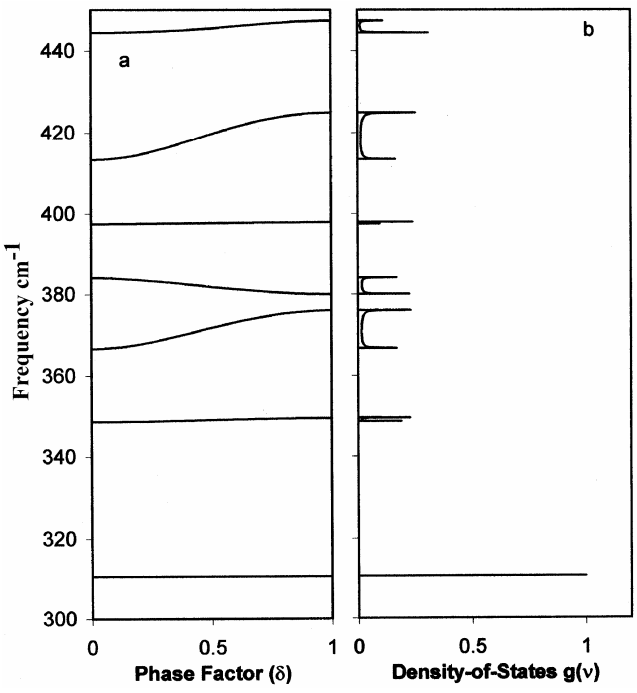

Fig. 5—Dispersion curves (a) and density-of-states (b) of poly (I) (300-450 cm^{-1})

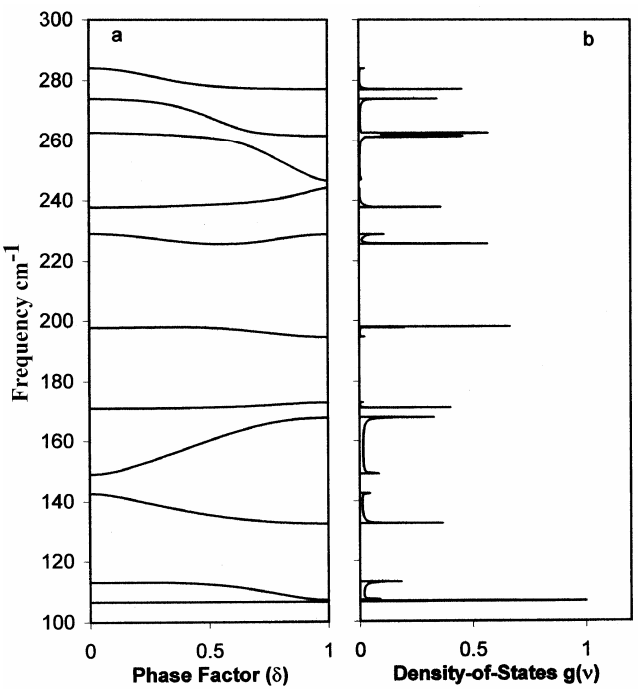

Fig. 6—Dispersion curves (a) and density-of-states (b) of poly (I) (100-300 cm^{-1})

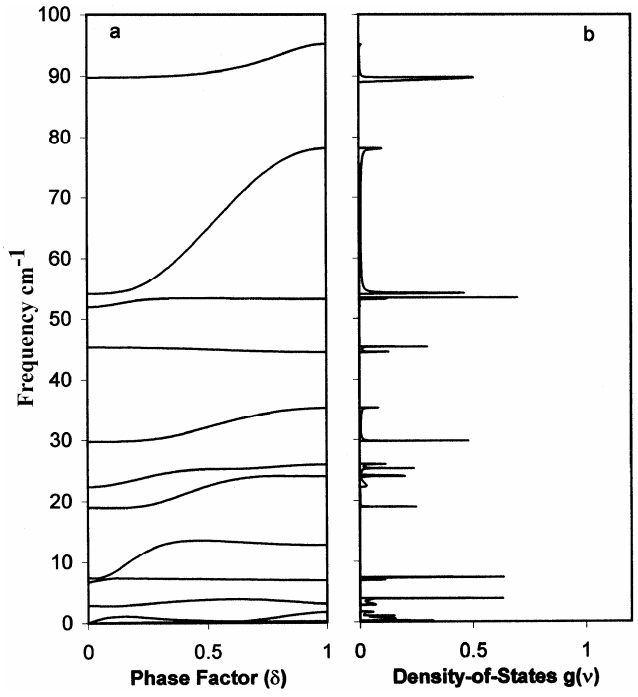

Fig. 7—Dispersion curves (a) and density-of-states (b) of poly (I) (0-100 cm^{-1})

Table 2—Backbone and side chain modes of poly (I)
[All frquencies are in cm^{-1}]

Cal.	Obs.	Assignments (% potential energy distribution)
Backbone modes		
1643	1641	ν(C3'O)(80) +ν(CC)s(10)
1233	1234/1235^{+}	ν(P=O)(67) +ν(C2'O)(14)
1133	1135*	ν(C5'C4')(58) +ν(CC)s(19)
1101	1100/1087^{+}	ν(P=O)(88)
918	918*	ν(C4'/C1',O4')(40)
872	879*	ν(OC5')(62) +ν(P-O)(15)
819	812*/814^{+}	ν(P-O)(39) +ν(CC)s(16) + ϕ(O-P=O)(10)
794	785*/790^{+}	ν(CC)s(22) +ν(P-O)(18) + ν(C4'/C1',O4')(14) + ϕ(O-P=O)(12)
752	762	ν(P-O)(38) + ν(CC)s(16)
683	683	ϕ(O-P=O)(15)
632	628	ϕ(O-P=O)(20)
621	611	ϕ(O=P=O)(35) + ϕ(O-P-O)(10)
582	579	ϕ(O-P=O)(35) + ϕ(C2'C1'N9)(11)
554	552*	ϕ(O4'C4'C3')(17) + ϕ(O-P=O)(16)
492	486	ϕ(O-P-O)(36) +ϕ(O-P=O)(23)
413		ϕ(O-P=O)(14) + ν(OC5')(12) + ν(P-O)(11)
384		ϕ(C5'C4'C3')(14) + ν(P-O)(10)
367		ω(C2'O)(23) + ϕ(C4'C3'C2')(12) +ϕ(C5'C4'C3')(11)
263		ϕ(C3'/C1'C2'O)(11) + ϕ(O-P=O)(10)
198		ϕ(POC5')(24) + τ(P-O)(20) + ϕ(O-P=O)(10)
149		τ(P-O)(22) + ϕ(C3'OP)(19) + τ(C3'O)(13)
22		ϕ(N9C1'O4')(11) + ϕ(C5'C4'C3')(11)
Side chain modes		
1715	1706*	ν(C6O6)(62) + ν(C6N1)(10)
1594	1596/1586^{+}	ν(C4C5)i(55) +ν(NC)i(14) +ν(C6O6)(14)
1396	1389/1381^{+}	ν(NC)i(37) +ν(C5C6)i(19) +ν(C6N1)(17)
1352	1341	ν(NC)i(41) +ν(C6N1)(19) + ν(C2N1)(17)
1260	1256/1262^{+}	ν(NC)i(33) +ν(C2N1)(36)
1148	1145/1153^{+}	ν(NC)i(36) +ν(C6N1)(20) +ν(N7C8)(17)
745	740	ϕ(N1C2N3)(18) + ϕ(C5N7C8)(13) +ϕ(C2N3C4)(13) + ν(NC)i(13) + ϕ(C6N1C2)(11)
444		ϕ(C5C6N1)(15) + ϕ(C2N3C4)(11)
398		ω(C6O6)(36) + τ(N1C2)(18) + τ(C6N1)(17) + τ(N7C8)(14) + τ(N9C4)(11)
310		ω(C6O6)(33) + τ(N9C4)(29) + τ(N7C8)(27)

* Frequencies in derivative spectra, $^{+}$ in Raman spectra

between some neighbouring modes (Table 4). These modes are close together at δ=0.0 and with increasing δ they fan out towards the zone boundary appearing to repel each other. For example, the two modes (149 and 143 cm^{-1}) are separated by only six wave numbers at the zone centre, but with increasing δ value they start diverging and finally, they are separated by 35 cm^{-1} at the zone boundary. It is interesting to note that similar to polyG[34] both modes disperse equally from their zone centre position, though in opposite direction. The nature of dispersion clearly indicates symmetry playing an important role. The potential energy of two modes is found predominantly in the skeletal modes and in addition, there is a diad axis

Table 3—Mix modes of poly (I)
[All frequencies are in cm^{-1}]

Cal.	Obs	Assignments (% P. E. D. at δ=0.0)	Cal.	Obs.	Assignments(% P. E. D. at δ=0.18π)
1230	1234/1235+	ν(C2'O)(43) + ν(P=O)(19) +ν(CC)s(10)	1230	1234/1235+	ν(C2'O)(43) + ν(P=O)(20) +ν(CC)s(15)
1186	1181	ν(N9,C1'/C8)(49)	1186	1181	ν(N9,C1'/C8)(49)
1064	1073	ν(N7C8)(21) +ν(NC)i(19) +ν(N9,C1'/C8)(17)	1064	1073	ν(N7C8)(21) +ν(NC)i(19) +ν(N9,C1'/C8)(17)
1051	1048/1042*	ν(N9,C1'/C8)(27) +ν(N7C8)(29) +ν(CC)s(13)	1051	1048/1042*	ν(N9,C1'/C8)(27) +ν(N7C8)(29) +ν(CC)s(13)
997	1000/1000*	ν(CC)s(43) +ν(N7C8)(11)	997	1000/1000*	ν(CC)s(43) +ν(N7C8)(11)
967	976/972*	ν(N7C8)(31) + ν(C4'/C1',O4')(14)	967	976/972	ν(N7C8)(31)+ν(C4'/C1',O4')(14)
939	935	ν(C4'/C1',O4')(44) +ν(N7C8)(22) +ν(N9,C1'/C8)(10)	939	935	ν(C4'/C1',O4')(44) + ν(N7C8)(22) + ν(N9,C1'/C8)(10)
894	897	ν(C4'/C1',O4')(32) +ν(N9,C1'/C8)(13) +ν(CC)s(10)	894	897	ν(C4'/C1',O4')(32) +ν(N9,C1'/C8)(13) + ν(CC)s(10)
648	651	ϕ(O-P=O)(17) + ϕ(C2'C1'N9)(13)	649	651	ϕ(O-P=O)(17) + ϕ(C2'C1'N9)(13)
613	611	ϕ(O-P=O)(15)	611	611	ϕ(O-P=O)(16)
597	595	ϕ(C5C6O6)(13) + ϕ(O-P=O)(13)	596		ϕ(O-P=O)(15) + ϕ(C5C6O6)(13)
525	524	ϕ(O-P=O)(30)	525	524	ϕ(O-P=O)(30)
472		ϕ(O-P=O)(15) + ν(CC)s(11)	471		ϕ(O-P=O)(14) + ν(CC)s(10)
459		ϕ(C3'/C1'C2'O)(18) + ω(C2'O)(17)	459		ϕ(C3'/C1'C2'O)(18) + ω(C2'O)(16)
348		ν(P-O)(11)	349		ν(P-O)(11) + ν(C5C6)i(11)
284		ϕ(C4'/C2'C3'O)(10) + ϕ(O-P=O)(8) + ϕ(POC5')(9)	283		ϕ(C4'/C2'C3'O)(9) + ϕ(C3'/C1'C2'O)(8) + ϕ(POC5')(8)
		ϕ(C3'/C1'C2'O)(8)			ϕ(O-P=O)(8)
274		τ(N7C8)(26) +τ(N9C4)(17)	274		τ(N7C8)(25) +τ(N9C4)(16)
238		τ(N9C4)(16) + τ(N7C8)(10)	238		τ(N9C4)(16) + τ(N7C8)(10)
229		ϕ(N9C1'O4')(11) + ϕ(C2'C1'N9)(10)	228		ϕ(N9C1'O4')(11) + ϕ(C2'C1'N9)(10)
171		τ(N9C4)(34) + τ(N1C2)(20) + τ(N7C8)(20)	171		τ(N9C4)(34) + τ(N1C2)(20) + τ(N7C8)(20)
143		ϕ(O4'C4'C3')(13) + τ(C3'O)(10)	141		τ(C3'O)(11) + ϕ(OCC)s(11)
113		ϕ(C4'C3'C2')(12) + τ(P-O)(11)	113		ϕ(C4'C3'C2')(11) + τ(P-O)(12)
107		τ(C5C6)(29) + τ(C6N1)(26) + τ(N9C4)(15)	107		τ(C5C6)(29) + τ(C6N1)(26) + τ(N9C4)(15)
90		ϕ(C2'C1'N9)(21) + τ(C1'N9)(14) + τ(N9C8)(10)	90		ϕ(C2'C1'N9)(21) +τ(C1'N9)(13) + τ(N9C8)(10)
54		τ(C4C5)(22) + τ(C1'N9)(13)	55		ϕ(C4'/C2'C3'O)(18) + τ(C4C5)(13) + ϕ(C3'OP)(10)
52		ϕ(C4'/C2'C3'O)(19)+τ(C1'N9)(16)+ϕ(C3'OP)(15)		53	τ(C1'N9)(25) + τ(C4C5)(12)
		τ(P-O)(11)			
45		τ(C4C5)(41) + ϕ(C4'C3'C2')(15)	45		τ(C4C5)(40) + ϕ(C4'C3'C2')(15)
30		τ(N9C4)(31) + τ(C5C6)(10)	30		τ(N9C4)(31) + τ(C5C6)(10)
19		τ(P-O)(11) + ϕ(C5'C4'C3')(10)	19		τ(P-O)(10) + ϕ(C5'C4'C3')(11)

* Frequencies in derivative spectra; + in Raman spectra; P.E.D., potential energy distribution

along the sugar-phosphate backbone. These symmetry elements are mainly responsible for the divergent dispersive behaviour.

Some pairs of modes show the opposite behaviour.

They are far separated at the zone centre, but move closer at the zone boundary. For example, a pair of modes calculated at 794 and 752 cm^{-1} shows such behaviour. These modes are backbone modes throughout the dispersion, having predominantly the PED of ν(P-O) + ν(CC)s. Another pair of modes

Table 4—Pair of modes showing specific features of dispersion curves

Freq. (δ = 0.0)	Before exchange				After exchange			
	δ/π	Freq.	P.E.D.	δ/π	Freq.	P.E.D.	δ/π	Freq.	P.E.D.
794	0.18	793	ν(CC)s(21) + ν(P-O)(19) + ν(C4′/C1′,O4′) (13) + ϕ (O-P=O)(12)	0.54	789	ν(P-O)(25) + ν(CC)s(20) + α(O-P=O)(13) + ν(C4′/C1′,O4′) (10)	1.0	782	ν(P-O)(30) + ν(CC)s(17) + α(O-P=O)(16)
752		753	ν(P-O)(38) + ν (CC)s(17)		760	ν(P-O)(37) + ν(CC)s(18)		770	ν(P-O)(37) + ν(CC)s(21)
745		745	ϕ (N1C2N3)(18) + ϕ (C5N7C8)(13) + ϕ(C2N3C4)(13) + ν(NC)i(12) + ϕ(C6N1C2)(10)		745	α(N1C2N3) (17) + α(C5N7C8)(14) + ν(NC)i (12) + α (C2N3C4)(12) + α(C6N1C2)(10)		745	α(N1C2N3) (17) + α(C5N7C8) (14) + ν(NC)i (12) + α(C2N3C4)(12) + α(C6N1C2)(10)
612	0.18	611	ϕ(O-P=O)(16)	0.54	606	α(O-P=O)(13) + α(C5C6O6)(11) α(C5C6O6)(11) α(O-P=O)(30)	0.72	604	α(C5C6O6)(15) +α(O6C6N1)(12)
597		596	ϕ(O-P=O)(15) + α(C5C6O6)(13)		595	α(O-P=O)(27) + α(OCC)s(12) +		594	α(O-P=O)(42)
582		583	ϕ(O-P=O)(34) + α(C2′C1′N9)(11)		585	α(C2′C1′N9)(12)		585	α(O-P=O)(24) + α(OCC)s(14) + α(C2′C1′N9)(13)
384	0.18	384	ϕ(C5′C4′C3′)(14)	0.54	382	α(C5′C4′C3′)(10)	0.72	381	ω(C2′O)(8) + α(O-P=O)(8) + α(C5′C4′C3′) (8) + α(C1′O4′C4′)(7)
366		368	ω(C2′O)(23) + α(CCC)s(11) + ϕ(C5′C4′C3′)(11)		372	ω(C2′O)(22) + α(C5′C4′C3′)(10)		375	ω(C2′O)(20) + α(C5′C4′C3′)(11)
274	0.36	272	τ(N==C)(17) + τ(N9C4)(11)	54	267	ν(P-O)(8) + α(POC5′) (8)	1.0	262	α(C3′/C1′C2′O)(11) + ν(P-O)(9)
263		262	ϕ (C3′/C1′C2′O)(12) + ϕ(O-P=O)(11)		261	α(O-P=O)(14) + α(C3′/C1′C2′O)(11) + α(C3′OP) (11)		247	α(POC5′)(15) + τ(N9C4)(9)
238		238	τ(N9C4)(17) + τ(N==C)(10)		239	τ(N9C4)(17) + τ(N==C)(11)		244	α(POC5′)(14) + α(C4′/C2′C3′O)(11) + α(O-P=O)(10)
149	0.18	152	τ(P-O)(17) + α(C3′OP)(15) + τ(C3′O)(11)	0.54	161	α(POC5′)(12) + τ (P-O)(10) + α(OC5′C4′)(9) +	1.0	168	τ (N9C4)(15) + α(POC5′)(12)+
143		141	τ(C3′O)(11) + ϕ (OCC)s(11)		135	α(OCC)s(10) + τ(C3′O)(9) + α(C1′N9C4)(9)		133	α(C1′N9C4)(11) + α(OCC)s(10) + α(N9C1′O4′)(9) + τ(C1′N9)(9)
30	0.18	30	τ(N9C4)(31) + τ(C5C6)(10)	54	33	τ(N9C4)(24)+ α(C5′C4′C3′)(11)	1.0	35	τ(N9C4)(16) + α(C4′/C2′C3′O)(11)
22		23	ϕ (N9C1′O4′)(10) + ϕ (C5′C4′C3′)(10) + ϕ (C4′/C2′C3′O) (9)		25	τ(P-O)(15) + α(N9C1′O4′)(12) + τ(C1′/C4′O4′)(10) + α(OCC)s(10)		26	τ(N9C4)(15) + τ(C5′C4′)(15) + α(N9C1′O4′)(10)
19		19	ϕ (C5′C4′C3′) (11) + τ(P-O)(10)		23	τ(P-O)(14) + τ(N9C4)(13) + τ(C5′C4′)(11)		24	α(C4′/C2′C3′O)(18) + τ(P-O)(17) + α(C3′OP)(14)

calculated at 384 and 366 cm^{-1} again pure backbone modes also shows similar behaviour. Earlier, in a preliminary study on poly(G)[33], such behaviour was also observed among the pair of modes calculated at 780 and 752 cm^{-1} and 385 and 365 cm^{-1}.

Another specific feature of the dispersion curves is the repulsion and mixing of the character of various pairs of modes (Table 4). The mixing of characters depends on the strength of repulsion and the stronger repulsion brings them closer and causes better exchange of character. This feature is observed between the modes calculated at 274, 263 and 238 cm^{-1} at the zone center. The 274 cm^{-1} mode is calculated as a mix mode at $\delta = 0.0$, showing a dominant PED from τ(N==C)(27) + τ(N9C4)(17) and a small contribution from the τ(C1'N9)(7). The 263 cm^{-1} is a pure backbone mode, with the PED ϕ(C3'C2'O)(11) + ϕ(O-P=O)(10) + ν(P-O)(9) + ν(CC)s(9) + ϕ(C3′OP)(8) + ϕ(CCC)s(7) + ϕ(C5′C4′O4′)(6)). The 238 cm^{-1} is again a mix mode having dominant PED from side chain vibrations τ(N9C4)(16) + τ(N=C)(9) + τ(N9C8)(8) and very small contributions from backbone vibrations ϕ(OC5'C4')(5) + ϕ(C2′C1′N9)(5). A mild exchange of character in the neighbourhood of $\delta = 0.54\ \pi$ is observed between the two modes appearing at 274 and 263 cm^{-1} ($\delta = 0.0$) which is an internal symmetry point (0.54 π is an integral multiple of 0.18 π). At this δ value, the 274 cm^{-1} mode becomes predominantly a backbone mode, with only 6% contribution from τ(N==C) character. Finally, at $\delta = 1.0\ \pi$, the τ(N==C) character is totally lost from the highest and lowest modes and only 7% contribution appears in the mid mode. From the observation of PED, it is clear that the τ(N==C) character is transferred to the previous higher mode, which was calculated at 283 cm^{-1} at the zone center. Similar exchange of character is observed among the modes calculated at 30, 22 and 19 cm^{-1}.

Heat capacity

The dispersion curves obtained for poly(I) have been used to calculate the density-of-states and heat capacity (C_p) as a function of temperature. The density-of-states are shown in Figs 4(b), 5(b), 6(b) and 7(b) respectively. Predictive values of C_p as a function of temperature are shown in Fig. 8. The purely skeletal and side chain and the mix modes of the two are given in Tables 2 and 3 respectively. It is clear from the Fig. 8 that the major contribution to the

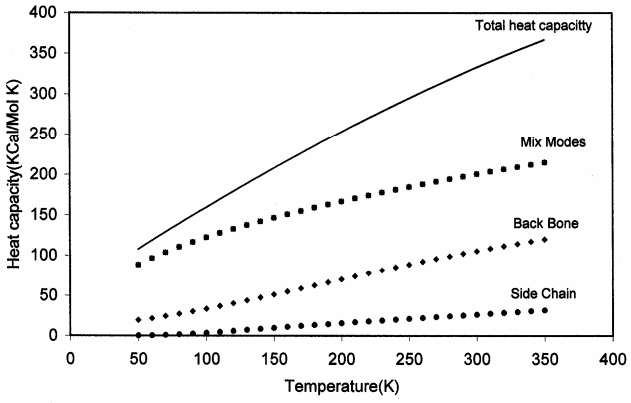

Fig. 8—Variation of heat capacity (C_p) with temperature

C_p comes from the backbone and side chain coupled modes.

It may be added here that the contribution from the lattice modes is bound to make a difference to the C_p due of its sensitivity to low frequency modes. However, so far we have solved the problem only for an isolated chain. The calculation of dispersion curves for a three dimensional system is extremely difficult. Inter-chain modes, involving hindered translatory and rotatory motions would appear and the total number of modes would depend on the contents of the unit cell. In systems, such as poly(I), the number of atoms in Unit cell is very large (nearly 242 in a single chain and there can be four such chains on the unit cell. This in turn makes the dimentions of the secular equation extremly large (>3 times). In addition, the number of interactions become enormous and some of them difficult even to visualize and quantify. The problem thus becomes almost intractable. The inter-chain interactions which are generally of the same order of magnitude as the weak intra-chain interactions would contribute to lower frequencies. Their introduction would, at best bring about crystal field splittings at the zone center or zone boundary, depending on the symmetry-dependent selection rules. However, the intra-chain assignments would remain by and large undisturbed. Thus, in spite of several limitations involved in the calculation of specific heat, the present work provides a good starting point for further basic studies on thermodynamic behaviour of polynucleotides, which go into well-defined conformations. Complete 3-D studies have been reported only on polyethylene, polyglycine, etc., where the unit cell is small. Other calculations with approximate inter-chain interactions as in a β sheet of polypeptides are confined to

calculations of zone centre and zone boundary frequencies alone by considering short segments. The present work goes beyond it and calculates the dispersion curves within the entire zone.

Conclusion

Dispersion curves obtained for poly(I) using Urey-Bradley force field provide a much better interpretation of IR absorptions and Raman spectra. Specific features in the dispersion, such as repulsion and exchange of character are observed at internal symmetry points with energy-momentum space corresponding approximately to integral multiples of helix angle.

Acknowledgement

Financial assistance to Seema Srivastava from the Department of Science and Technology, New Delhi under the Fast Track Scheme for Young Scientists) and Shinoo Srivastava (Research Associate) from Council of Scientific and Industrial Research, New Delhi is gratefully acknowledged.

References

1 Hobza P & Sponer J (1999) *J Chem Rev* 99, 3247-3276
2 Cheong C & Moore P B (1992) *Biochemistry* 31, 8406-14
3 Ridoux J P, Liquier J & Taillandier E (1988) *Biochemistry* 27, 3874-3878
4 Vives M, Gargallo R, Tauler R & Moreno V, (2001*) J Inorg Biochem* 85, 279-290
5 Taillandier E, Ridoux J P, Liquier J, Leupin W, Denny WA, Wang Y, Thomas G A & Peticolas W L (1987) *Biochemistry* 26, 3361-3368
6 Wang Y & Patel D J (1992) *Biochemistry* 31, 8112-8119
7 Srivastava S, Srivastava S, Singh S, Gupta V P & Gupta V D (2001) *J Macromol Sci – Phys* B40, 1-14
8 Lu K C, Prohofsky E W & Vanzandt L L (1977) *Biopolymers* 16, 2491-506
9 Prescott B, Steinmetz W & Thomas Jr G J (1984) *Biopolymers* 23, 235-56
10 Stefl R, Spackova N, Berger I, Koca J & Sponer J (2001) *Biophysical J* 80, 455-468
11 Barry D S & Dexter S Moore (1998) *Biophysical J* 74, 2249-2258
12 Pack G R, Prasad C V, Salafsky J S & Wong L (1986) *Biopolymers* 25, 1697-1715
13 Srivastava S, Gupta V D,Tandon P, Singh S & Katti S B (1999) *J Macromol Sci -Phy* B38, 349-66
14 Akeson M, Branton D, Kasianowicz J J, Brandin E & Deamer D W (1999*) Biophys J* 77, 3227-3233
15 Hua X M & Prohofsky E W (1988) *Biopolymers* 27, 645-655
16 Taddei P, Tinti A & Fini G (2001) *J Raman Spectroscopy* 32, 619-629
17 Srivastava S, Srivastava S, Singh S, Gupta V D & Gupta V P (2002) *Eur Polym J* 38, 1423-1434
18 Srivastava S, Tandon P, Gupta V D & Rastogi S (1996) *Polymer (UK)* 37, 5401-5410
19 Burman L, Tandon P, Gupta V D, Rastogi S & Srivastava S (1996) *Biopolymers* 38, 53 - 67
20 Srivastava S, Srivastava S, Melkani G C, Singh S, Gupta V D & Gupta V P (2002) *Indian J Biochem Biophys* 39, 410-418
21 Simard C & Savoie R (1994) *Biopolymers* 34, 91-100
22 Arnott S, Chandrasekaran R & Marttila C M (1974) *Biochem J* 141, 537-543
23 Cech C L & Tinoco I, (1976) *Nucleic Acids Res* 3, 399-404
24 Brown K G, Kiser E J & Peticolas W L (1972) *Biopolymers* 11, 1855-1869
25 Chou C H, Thomas G J Jr, Arnott S & Campbell Smith P J (1977) *Nucleic Acids Res* 4, 2407 - 2419
26 Reddy S Y, Fabrice Lecler C & Karplus M, (2003) *Biophys J* 84, 1421-1449
27 Wilson E B, Decius J C & Cross P C (1980) *Molecular Vibrations: The Theory of Infrared and Raman Vibrational Spectra*, Dover Publications, NewYork
28 Higgs P W (1953) *Proc Roy Soc (London)* A220, 472
29 Tandon P, Gupta V D, Prasad O, Rastogi S & Gupta V P (1997) *J Polym Sci Part B: Polymer Phys* 35, 2281-2292
30 King W T, Mills I M, Crawford B L (1957) *J Chem Phys* 27, 455
31 Benzinger T H (1971) *Nature* 229, 100
32 Pan R, Verma-Nair M, & Wunderlich B (1989) *J Therm Anal* 35, 955
33 Perutz M F (1962) *Proteins & Nucleic Acid: Structure and Function*, Elsevier Publications, New York
34 Srivastava S, Srivastava S, Singh, S, Gupta V P & Gupta V D (2003) *Eur Polym J* 39, 341-354